

Effects of thermal treatment on organic-inorganic hybrid perovskite films and luminous efficiency of light-emitting diodes

Young-Hoon Kim ^a, Himchan Cho ^a, Jin Hyuck Heo ^b, Sang Hyuk Im ^b, Tae-Woo Lee ^{a,*}

^a Department of Materials Science and Engineering, Pohang University of Science and Technology, Pohang 790-784, Republic of Korea

^b Department of Chemical Engineering, College of Engineering, Kyung Hee University, 1 Seochon-dong Giheung-gu, Yongin-si, Gyeonggi-do 446-701, Republic of Korea



ARTICLE INFO

Article history:

Received 14 January 2016

Received in revised form

14 May 2016

Accepted 2 June 2016

Available online 7 June 2016

Keywords:

Thermal treatment

Crystallinity

Organic-inorganic perovskite

Light-emitting diodes

Luminous efficiency

ABSTRACT

To improve the electroluminescence efficiency of organic-inorganic hybrid perovskite (OIP) films, we need to consider several different types of post-treatments after film formation such as thermal annealing and solvent annealing. Here, we only applied thermal treatment on the film excluding all the other treatments. Then, we analyzed the effects of annealing time t_{ann} on crystallinity of methylammonium lead bromide ($\text{CH}_3\text{NH}_3\text{PbBr}_3$) films and on luminous efficiency of $\text{CH}_3\text{NH}_3\text{PbBr}_3$ -based perovskite light-emitting diodes (PrLEDs). When thermal annealing of $\text{CH}_3\text{NH}_3\text{PbBr}_3$ films was conducted at 90°C , $t_{\text{ann}} \leq 10$ min increased its crystallinity by eliminating residual solvent and completing the conversion of precursor to crystal, but $t_{\text{ann}} > 10$ min reduced crystallinity and caused slight sublimation of $\text{CH}_3\text{NH}_3\text{Br}$. This was consistent with trend of the luminous efficiency of our PrLEDs that showed the optimum performance at $t_{\text{ann}} = 10$ min. These results demonstrate that optimizing t_{ann} of $\text{CH}_3\text{NH}_3\text{PbBr}_3$ films is a simple way to improve the luminous efficiency of PrLEDs by controlling their crystallinity.

© 2016 Elsevier B.V. All rights reserved.

Organic/inorganic hybrid perovskite (OIP) materials can attain power conversion efficiency > 20% due to their unique properties such as small exciton binding energy (<50 meV), long exciton diffusion length (>100 nm) and high absorption coefficient so that they have possible applications in the light-absorption layers of solar cells [1–6].

OIPs also have potential applications as emitters in light-emitting diodes (LEDs) because the emitting materials are inexpensive, processing can be done at low cost, and the emitting spectrum is very narrow (full width at half maximum (FWHM) ≤ 20 nm) [7,8]. Also, their easy band-gap tunability by simple atom substitutions of organic cations [9,10], inorganic anions [11] and metal cations [12], and independence of color purity on crystal size [13,14] make them feasible in alternative emitters that do not have the disadvantages of conventional organic emitters (e.g. low color-purity, complex synthesis and high cost), and inorganic quantum-dot (QD) emitters (e.g. color purity easily affected by crystal size, high cost and finely controlled synthesis) [15,16]. Although excitons in OIP films can be easily dissociated by thermal ionization, OIP

films can be converted to bright emitters by controlling charge injection barrier and exciton quenching at the interface between OIP and adjacent hole/electron injection layer [17–20]. However, controlling several factors in forming the OIP layer that are strongly related to the photoluminescence quantum efficiency (PLQE) of OIPs and luminous efficiencies of OIP based LEDs should be done carefully.

Electroluminescence (EL) of OIPs can be affected by the imperfect crystallization caused by residual solvent, and by incomplete conversion of precursor to crystal in the OIP film [21,22]. To make better poly-crystal films for devices, several different types of post-treatments such as thermal annealing and solvent annealing can be applied [22,23]. When OIP is not thermally annealed or annealed too short, the film has low crystallinity which can decrease its PLQE by reducing radiative recombination and increasing non-radiative recombination [24]. Thus, to increase the EL and PLQE of the OIPs, thermal treatment after film formation must be used to increase the crystallinity by reducing residual solvent and converting remaining precursors to crystal (Fig. 1). However, thermal treatment for too long induces sublimation of organic ammonium from the perovskite film and reduces the crystallinity [25]. Thus, to increase the luminous efficiencies of perovskite-based LEDs (PrLEDs),

* Corresponding author.

E-mail addresses: twlee@postech.ac.kr, taewlees@gmail.com (T.-W. Lee).

the OIP needs to have perfect crystallinity without residual solvent, and the precursor need to be completely converted to crystal, in addition, sublimation of organic ammonium by thermal treatment must be avoided by adjusting annealing duration t_{ann} .

Here, we used X-ray diffraction (XRD) measurements and X-ray photoelectron spectroscopy (XPS) measurements to analyze how thermal annealing affects perovskite films and the luminous efficiencies of PrLEDs that use them without any other chemical treatments such as solvent annealing process and nano-crystal pinning process [8]. We chose $\text{CH}_3\text{NH}_3\text{PbBr}_3$ as an emitting layer (EML) because it has higher exciton binding energy (76–150 meV), shorter exciton diffusion length (~ 100 nm) at room temperature (RT) and more stable cubic phase [17,26] than do other perovskite materials (e.g. 2–50 meV, ~ 50 nm and distorted cubic phase for exciton binding energy, exciton diffusion length and crystal structure respectively of $\text{CH}_3\text{NH}_3\text{PbI}_3$ at RT) [27,28]. We used the self-organized buffer hole injection layer (Buf-HIL) composed of poly(3,4-ethylenedioxythiophene):poly(styrene sulfonate) (PEDOT:PSS) and perfluorinated polymeric acid, tetrafluoroethylene-perfluoro-3,6-dioxa-4-methyl-7-octene-sulfonic acid copolymer (PFI) to facilitate the hole injection to the OIP EML and prevent the exciton quenching at the interface [17,29–31].

1. Experimental details

To synthesize $\text{CH}_3\text{NH}_3\text{Br}$, we reacted 50 ml hydrobromic acid (Sigma-Aldrich Inc.) (45 wt% in water) and 30 ml methylamine (Junsei Chemical Co. Ltd) (40 wt% in methanol) in a 250-ml round-bottom flask for 2 h under vigorous stirring at 0 °C. After the reaction was finished, we evaporated all solvents by heating the solution at 50 °C for 1 h in vacuum. We collected the residual precipitates and purified them by dissolving in ethanol, recrystallizing from diethyl ether, and drying at RT in a vacuum oven for 24 h.

To fabricate the PrLEDs, we sonicated the ITO-patterned glass in acetone and in 2-isopropanol for 15 min, respectively, and then boiled the clean glass in 2-isopropanol for 30 min. Then, we UV-ozone treated the cleaned ITO glass for 10 min to remove residual organic molecules, and to make the surface hydrophilic. On the cleaned glass, Buf-HIL solution composed of PEDOT:PSS mixed with PFI solution (1:1 w:w) was filtered through a 0.45-μm polyvinylidene difluoride (PVDF) syringe filter, then spin coated at 4500 rpm for 90 s to give a 40-nm thickness. The resulting Buf-HIL was annealed at 150 °C for 30 min in air to remove residual solvents. The sample was transferred to N_2 atmosphere in a glove box. $\text{CH}_3\text{NH}_3\text{PbBr}_3$ solution was prepared by mixing $\text{CH}_3\text{NH}_3\text{Br}$ and PbBr_2 (Sigma-Aldrich Inc.) (1:1 mol:mol) in *N,N*-dimethylformamide (DMF) (40% by wt), then spin-coated on the Buf-HIL at 3000 rpm for 90 s. The $\text{CH}_3\text{NH}_3\text{PbBr}_3$ layer has both scattered large particles (>1 μm) and thin uniform film (~ 100 nm). Then glass/ITO/Buf-HIL/ $\text{CH}_3\text{NH}_3\text{PbBr}_3$ samples were annealed by baking at 90 °C

for $t_{\text{ann}} = 0, 2, 5, 10, 20, 30$, or 60 min. After annealing, each sample were transferred to a thermal evaporator, then 1,3,5-Tris(1-phenyl-1*H*-benzimidazol-2-yl)benzene (TPBI) (50 nm), LiF (1 nm) and Al (100 nm) were deposited in sequence at 1 Å/s, 0.1 Å/s and 3 Å/s, respectively, under high vacuum ($<10^{-7}$ Torr). The pixel area of PrLEDs is 6 mm². The fabricated devices were encapsulated to maintain the N_2 condition, and current-voltage-luminance characteristics were measured using a Keithley 236 source measurement unit and a Minolta CS200 spectroradiometer.

2. Results and discussion

2.1. XRD analysis

We compared the XRD patterns of $\text{CH}_3\text{NH}_3\text{PbBr}_3$ layer annealed at 90 °C for different t_{ann} to quantify how t_{ann} affected the crystallinity of films. XRD patterns of all samples showed sharp diffraction peaks at $\sim 15.04^\circ$ for (100), $\sim 21.38^\circ$ for (110), $\sim 33.96^\circ$ for (210), $\sim 37.34^\circ$ for (211), $\sim 43.34^\circ$ for (220) and $\sim 46.12^\circ$ for (300) [32]. The XRD pattern about 10 min annealing is taken from our previous paper for comparison [17]. These peaks are consistent with previous reports and indicate that well-crystallized $\text{CH}_3\text{NH}_3\text{PbBr}_3$ layers with the α -axis self-assembly was fabricated (Fig. 2a) [33]. However, most XRD peak intensities tended to increase over $0 \leq t_{\text{ann}} \leq 20$ min (Fig. 2b–f). The remaining solvent in film after direct spin-coating induced imperfect conversion from $\text{CH}_3\text{NH}_3\text{PbBr}_3$ precursors to crystal, and yielded $\text{CH}_3\text{NH}_3\text{PbBr}_3$ layers with poor crystallinity [21,22]; annealing for $10 \leq t_{\text{ann}} \leq 20$ min increased this crystallinity by evaporating residual solvent (DMF).

The crystallite sizes L were calculated using the Scherrer equation ($L = \frac{K\lambda}{B \cos \theta}$ where $K = 0.94$ [dimensionless] is the Scherrer constant, $\lambda = 0.154$ [nm] is the X-ray wavelength, B is FWHM [radian] of an XRD peak and θ [radian] is X-ray angle). All L were similar to $25.7 \text{ nm} \pm 0.4 \text{ nm}$, which is smaller than the grain size ($>1 \mu\text{m}$) [34]; the difference indicates that the perovskite films are consisted of many crystalline domains. Thus, thermal annealing of OIP films can increase the PLQE and crystallinity by not only removing residual solvents and completing the conversion of precursor to crystals but also increasing the orientation uniformity of the perovskite crystalline domains.

However, XRD peak intensities decreased at $t_{\text{ann}} > 20$ min, possibly due to sublimation of $\text{CH}_3\text{NH}_3\text{Br}$ or decomposition to CH_3NH_2 and HBr from the crystal of $\text{CH}_3\text{NH}_3\text{PbBr}_3$ film during extended annealing. The sublimation or decomposition of $\text{CH}_3\text{NH}_3\text{Br}$ makes the non-stoichiometric molar ratio of $\text{CH}_3\text{NH}_3\text{Br}$ to PbBr_2 in $\text{CH}_3\text{NH}_3\text{PbBr}_3$, so this sublimation or decomposition can degrade the cubic phase crystal structure and reduce the XRD peak intensity. This result comes from the fact that when methylammonium halide ($\text{CH}_3\text{NH}_3\text{X}$; X is Cl or Br or I) and PbX_2 formed the perovskite structure ($\text{CH}_3\text{NH}_3\text{PbX}_3$), $\text{CH}_3\text{NH}_3\text{X}$ can be released

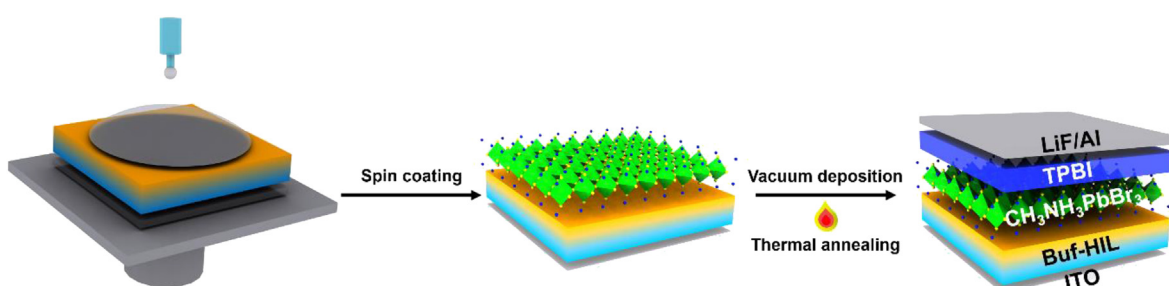


Fig. 1. Schematic illustrations of device fabrication.

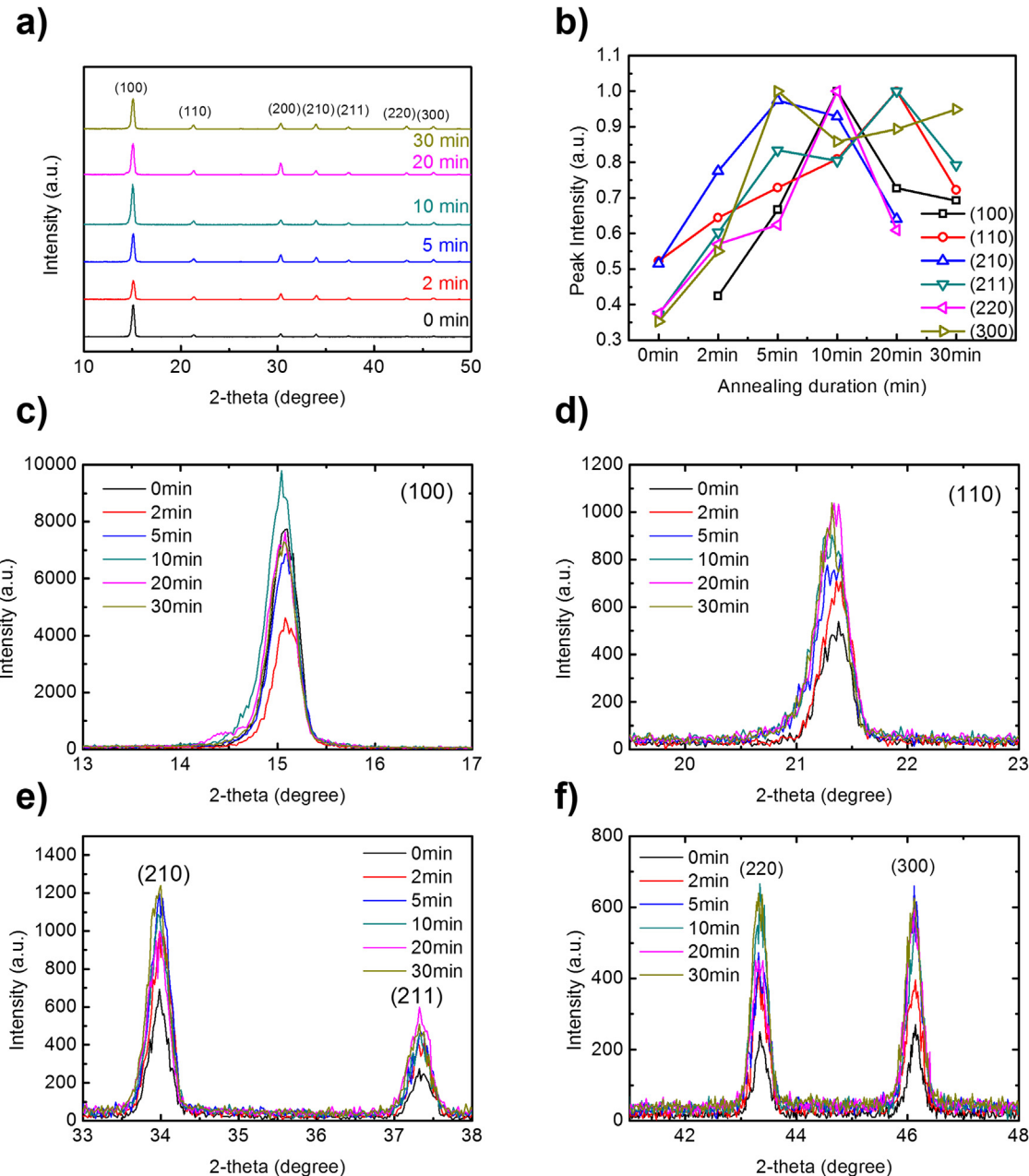


Fig. 2. a) Full XRD spectra, b) summary of XRD peak intensities of OIP films, c) (100) peaks, d) (110) peaks, e) (210) peaks and (211) peaks, f) (220) peaks and (300) peaks of OIP films with different annealing durations. The XRD pattern about 10 min annealing is taken from our previous paper for comparison [17].

from perovskite structure at lower temperature than the temperature when they exist as their individual components [25].

2.2. XPS analysis

To analyze the chemical changes and the sublimation of $\text{CH}_3\text{NH}_3\text{Br}$ from perovskite film according to the thermal annealing, we conducted the XPS of $\text{CH}_3\text{NH}_3\text{PbBr}_3$ samples at $t_{\text{ann}} = 0, 5, 10, 20, 30$ or 60 min (Fig. 3a–d). The full XPS spectra showed Br peaks (~68 eV), Pb peaks (~138 and 143 eV), C peaks (~285 eV) and N peaks (~400 eV) in all samples; these species clearly indicate the fabrication of $\text{CH}_3\text{NH}_3\text{PbBr}_3$. The XPS spectrum about 10 min annealing is taken from the Reference [17] for comparison. The N peak and Br peak areas increased slightly until $t_{\text{ann}} = 10$ min, possibly due to the increased exposure of perovskite surface as

residual solvent evaporated. The N and Br peaks decreased at $t_{\text{ann}} > 10$ min possibly due to the sublimation or decomposition of $\text{CH}_3\text{NH}_3\text{Br}$ from perovskite film because $\text{CH}_3\text{NH}_3\text{Br}$ can be easily released when it is mixed with PbBr_2 and forms $\text{CH}_3\text{NH}_3\text{PbBr}_3$ structure. Decreasing $[\text{N}]/[\text{Pb}]$ and $[\text{Br}]/[\text{Pb}]$ ratio at $t_{\text{ann}} > 10$ min also confirm the sublimation or decomposition of $\text{CH}_3\text{NH}_3\text{Br}$ from perovskite film (Fig. 3e and f). These sublimation of N and Br at $t_{\text{ann}} > 10$ min reduced the crystallinity of OIP films, which was confirmed by XRD data, and can limit the PLQE of OIPs and luminous efficiencies of PrLEDs (Fig. 4).

2.3. PrLED characteristics

To quantify how thermal annealing of the OIP film affects device efficiencies, we fabricated PrLEDs (ITO/Buf-HIL/ $\text{CH}_3\text{NH}_3\text{PbBr}_3$ /TPBI/

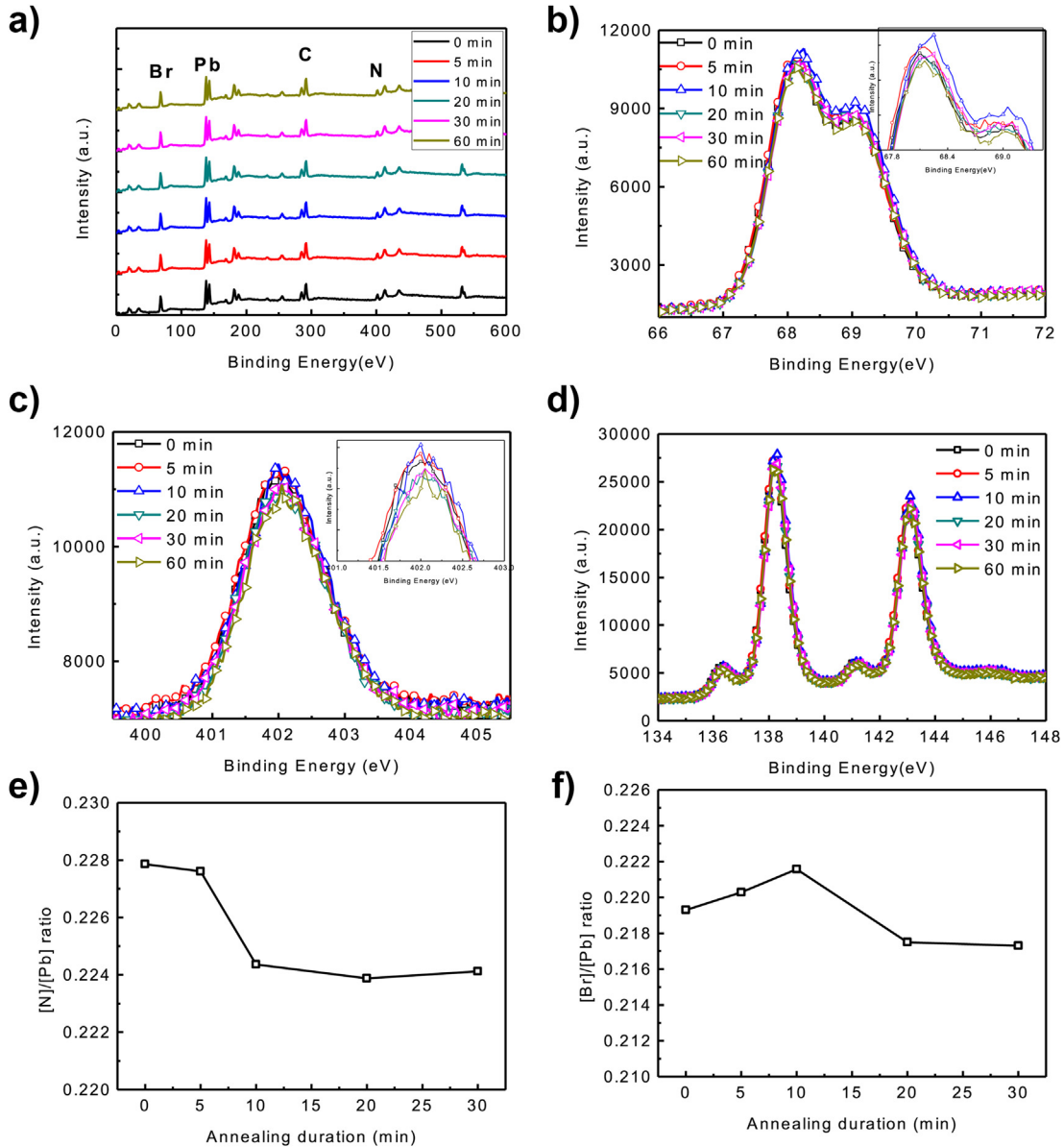


Fig. 3. a) Full XPS spectra, b) Br peaks XPS spectra, c) N peaks XPS spectra of OIP films with different annealing durations, d) Pb peaks XPS spectra, e) $[N]/[Pb]$ ratio and f) $[Br]/[Pb]$ ratio with OIPs with different annealing durations. The XPS spectrum about 10 min annealing is taken from the Reference [17] for comparison.

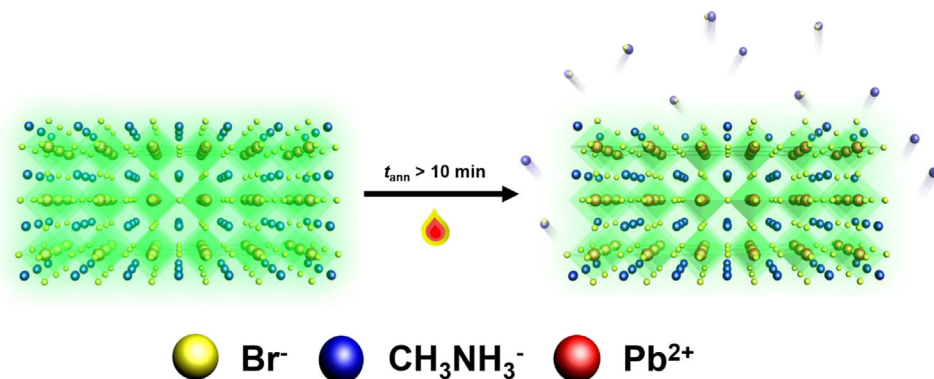


Fig. 4. Schematic illustrations of $\text{CH}_3\text{NH}_3\text{PbBr}_3$ film and sublimation or decomposition of $\text{CH}_3\text{NH}_3\text{Br}$ under thermal annealing treatment over 10 min.

LiF/Al) with $t_{\text{ann}} = 0, 5, 10, 20$ or 30 min (Fig. 5a). The luminous efficiency data of PrLEDs with 10 min annealed OIPs was obtained from the Reference [17] for comparison. PrLEDs with 10 -min annealed OIP film showed current efficiency (CE) $\sim 0.577 \text{ cd/A}$, external quantum efficiency (EQE) $\sim 0.125\%$ and maximum luminescence (ML) $\sim 417.28 \text{ cd/m}^2$, which are higher than those of the other devices (Fig. 5b–d and Table 1). Luminous efficiencies of PrLEDs tended to increase as t_{ann} increased from 0 min (CE $\sim 0.279 \text{ cd/A}$, EQE $\sim 0.06\%$ and ML $\sim 202.4 \text{ cd/m}^2$) to 10 min due to the increasing crystallinity of OIP film as a result of evaporation of residual solvent, complete conversion of precursor to crystal and increasing orientation uniformity of perovskite crystalline domains. However, at

$t_{\text{ann}} > 10$ min, PrLEDs showed gradually decreasing device efficiencies from CE $\sim 0.426 \text{ cd/A}$, EQE $\sim 0.092\%$ and ML $\sim 436.5 \text{ cd/m}^2$ (for $t_{\text{ann}} = 20$ min) to CE $\sim 0.323 \text{ cd/A}$, EQE $\sim 0.07\%$ and ML $\sim 113.52 \text{ cd/m}^2$ (for $t_{\text{ann}} = 30$ min); these decreases are attributed to the sublimation or decomposition of $\text{CH}_3\text{NH}_3\text{Br}$ from the OIP films. All devices showed the similar EL spectrum and Commission Internationale de l'Éclairage (CIE) coordinates ($0.278, 0.706$) which are located at the edge of CIE graph and indicate that color was very pure (Fig. 5e and f).

Our work shows that improving the crystallinity of OIP films by optimizing annealing duration is a very simple method to increase the luminous efficiencies of PrLEDs.

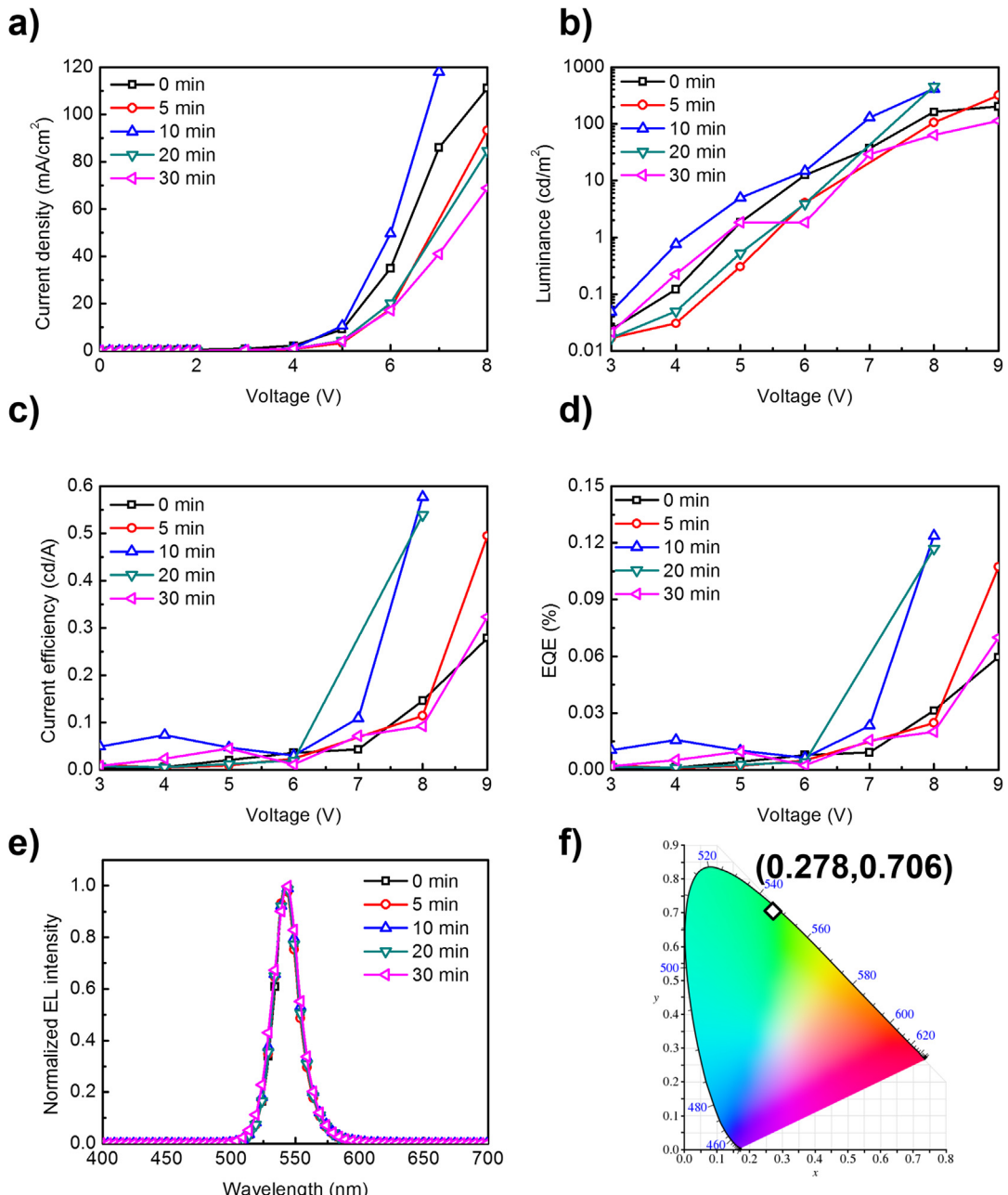


Fig. 5. a) Current density-versus-voltage spectra, b) luminance-versus-voltage spectra, c) current efficiency-versus-voltage spectra, d) EQE-versus-voltage spectra, e) EL spectra and f) CIE coordinates of PrLEDs with OIP annealed for different durations. The luminous efficiency data of PrLEDs with 10 min annealed OIPs were obtained from the Reference [17] for comparison.

Table 1

Maximum current efficiency, external quantum efficiency and luminance of PrLEDs using OIP films with different annealing durations.

Annealing duration [min]	Max CE (cd/A)	Max EQE (%)	Max luminance (cd/m ²)
0	0.279	0.060	202.40
5	0.495	0.107	319.94
10	0.577	0.125	417.28
20	0.426	0.092	436.51
30	0.323	0.070	113.52

3. Conclusion

In conclusion, we have analyzed the effect of thermal annealing on $\text{CH}_3\text{NH}_3\text{PbBr}_3$ films with XRD and XPS measurements. When thermal annealing was conducted on $\text{CH}_3\text{NH}_3\text{PbBr}_3$ films at 90 °C, $t_{\text{ann}} \leq 10$ min increased its crystallinity by eliminating residual solvent and completing the conversion of precursor to crystal, but $t_{\text{ann}} > 10$ min reduced crystallinity by causing slight sublimation or decomposition of $\text{CH}_3\text{NH}_3\text{Br}$. We found that trends of XRD and XPS results were very consistent with that of the devices efficiencies. We also fabricated PrLEDs with $\text{CH}_3\text{NH}_3\text{PbBr}_3$ films annealed at different duration and PrLEDs with $t_{\text{ann}} = 10$ min without using any other post-treatments showed the optimum efficiencies. Considering the trade-off between evaporating residual solvent and completing the conversion of precursor to crystal in $t_{\text{ann}} \leq 10$ min, and sublimation or decomposition of $\text{CH}_3\text{NH}_3\text{Br}$ in $t_{\text{ann}} > 10$ min, we determined that $t_{\text{ann}} = 10$ min maximized the crystallinity of perovskite film and luminous efficiencies of PrLEDs.

Acknowledgements

This research was supported by the Nano Material Technology Development Program through the National Research Foundation of Korea (NRF) funded by the Ministry of Science, ICT & Future Planning (MSIP, Korea) (NRF-2014M3A7B4051747).

References

- [1] W.S. Yang, J.H. Noh, N.J. Jeon, Y.C. Kim, S. Ryu, J. Seo, S.I. Seok, High-performance photovoltaic perovskite layers fabricated through intramolecular exchange, *Science* 348 (2015) 1234–1237.
- [2] N.J. Jeon, J.H. Noh, W.S. Yang, Y.C. Kim, S. Ryu, J. Seo, S.I. Seok, Compositional engineering of perovskite materials for high-performance solar cells, *Nature* 517 (2015) 476–480.
- [3] J.-H. Im, I.-H. Jang, N. Pellet, M. Grätzel, N.-G. Park, Growth of $\text{CH}_3\text{NH}_3\text{PbI}_3$ cuboids with controlled size for high-efficiency perovskite solar cells, *Nat. Nanotechnol.* 9 (2014) 927–932.
- [4] H. Kim, K.-G. Lim, T.-W. Lee, Planar heterojunction organometal halide perovskite solar cells: roles of interfacial layers, *Energy Environ. Sci.* 9 (2016) 12–30.
- [5] K.-G. Lim, S. Ahn, Y.-H. Kim, Y. Qi, T.-W. Lee, Universal energy level tailoring of self-organized hole extraction layers in organic solar cells and organic–inorganic hybrid perovskite solar cells, *Energy Environ. Sci.* 9 (2016) 932–939.
- [6] K.-G. Lim, S. Ahn, H. Kim, M.-R. Choi, D.H. Huh, T.-W. Lee, Self-doped conducting polymer as a hole-extraction layer in organic–inorganic hybrid perovskite solar cells, *Adv. Mater. Interfaces* 3 (2016) 1500678.
- [7] M. Era, S. Morimoto, T. Tsutsui, S. Saito, Organic-inorganic heterostructure electroluminescent device using a layered perovskite semiconductor ($\text{C}_6\text{H}_5\text{C}_2\text{H}_4\text{NH}_3)_2\text{PbI}_4$), *Appl. Phys. Lett.* 65 (1994) 676–678.
- [8] H. Cho, S.-H. Jeong, M.-H. Park, Y.-H. Kim, C. Wolf, C.-L. Lee, J.H. Heo, A. Sadhanala, N. Myoung, S. Yoo, S.H. Im, R.H. Friend, T.-W. Lee, Overcoming the electroluminescence efficiency limitations of perovskite light-emitting diodes, *Science* 350 (2015) 1222–1225.
- [9] T.M. Koh, K. Fu, Y. Fang, S. Chen, T.C. Sum, N. Mathews, S.G. Mhaisalkar, P.P. Boix, T. Baikie, Formamidinium-containing metal-halide: an alternative material for near-IR absorption perovskite solar cells, *J. Phys. Chem. C* 118 (2013) 16458–16462.
- [10] G.E. Eperon, S.D. Stranks, C. Menelaou, M.B. Johnston, L.M. Herz, H.J. Snaith, Formamidinium lead trihalide: a broadly tunable perovskite for efficient planar heterojunction solar cells, *Energy Environ. Sci.* 7 (2014) 982–988.
- [11] A. Kojima, K. Teshima, Y. Shirai, T. Miyasaka, Organometal halide perovskites as visible-light sensitizers for photovoltaic cells, *J. Am. Chem. Soc.* 131 (2009) 6050–6051.
- [12] D.B. Mitzi, Synthesis, crystal structure, and optical and thermal properties of $(\text{C}_4\text{H}_9\text{NH}_3)_2\text{Ml}_4$ ($\text{M} = \text{Ge}, \text{Sn}, \text{Pb}$), *Chem. Mater.* 8 (1996) 791–800.
- [13] Z.-K. Tan, R.S. Moghaddam, M.L. Lai, P. Docampo, R. Higler, F. Deschler, M. Price, A. Sadhanala, L.M. Pazos, D. Credgington, F. Hanusch, T. Bein, H.J. Snaith, R.H. Friend, Bright light-emitting diodes based on organometal halide perovskite, *Nat. Nanotechnol.* 9 (2014) 687–692.
- [14] G. Xing, N. Mathews, S.S. Lim, N. Yantara, X. Liu, D. Sabba, M. Grätzel, S. Mhaisalkar, T.C. Sum, Low-temperature solution-processed wavelength-tunable perovskites for lasing, *Nat. Mater.* 13 (2014) 476–480.
- [15] J. Kwak, W.K. Bae, D. Lee, I. Park, J. Lim, M. Park, H. Cho, H. Woo, D.Y. Yoon, K. Char, S. Lee, C. Lee, Bright and efficient full-color colloidal quantum dot light-emitting diodes using an inverted device structure, *Nano Lett.* 12 (2012) 2362–2366.
- [16] Y.-H. Niu, A.M. Munro, Y.-J. Chen, Y. Tian, M.S. Liu, J. Zhao, J.A. Bardecker, I.J.-L. Plante, D.S. Ginger, A.K.-J. Jen, Improved performance from multilayer quantum dot light-emitting diodes via thermal annealing of the quantum dot layer, *Adv. Mater.* 19 (2007) 3371–3376.
- [17] Y.-H. Kim, H. Cho, J.H. Heo, T.-S. Kim, N. Myoung, C.-L. Lee, S.H. Im, T.-W. Lee, Multicolored organic/inorganic hybrid perovskite light-emitting diodes, *Adv. Mater.* 27 (2015) 1248–1254.
- [18] J. Wang, N. Wang, Y. Jin, J. Si, Z.-K. Tan, H. Du, L. Cheng, X. Dai, S. Bai, H. He, Z. Ye, M.L. Lai, R.H. Friend, W. Huang, Interfacial control toward efficient and low-voltage perovskite light-emitting diodes, *Adv. Mater.* 27 (2015) 2311–2316.
- [19] R.L.Z. Hoye, M.R. Chua, K.P. Musselman, G. Li, M.-L. Lai, Z.-K. Tan, N.C. Greenham, J.L. MacManus-Driscoll, R.H. Friend, D. Credgington, Enhanced performance in fluorene-free organometal halide perovskite light-emitting diodes using tunable, low electron affinity oxide electron injectors, *Adv. Mater.* 27 (2015) 1414–1419.
- [20] J.C. Yu, D.B. Kim, G. Baek, B.R. Lee, E.D. Jung, S. Lee, J.H. Chu, D.-K. Lee, K.J. Choi, S. Cho, M.H. Song, High-performance planar perovskite optoelectronic devices: a morphological and interfacial control by polar solvent treatment, *Adv. Mater.* 27 (2015) 3492–3500.
- [21] Y. Tidhar, E. Edri, H. Weissman, D. Zohar, G. Hodes, D. Cahen, B. Rybtchinski, S. Kirmayer, Crystallization of methyl ammonium lead halide perovskites: implications for photovoltaic applications, *J. Am. Chem. Soc.* 136 (2014) 13249–13256.
- [22] A. Dualeh, N. Tétreault, T. Moehl, P. Gao, M.K. Nazeeruddin, M. Grätzel, Effect of annealing temperature on film morphology of organic–inorganic hybrid perovskite solid-state solar cells, *Adv. Funct. Mater.* 24 (2014) 3250–3258.
- [23] Z. Xiao, Q. Dong, C. Bi, Y. Shao, Y. Yuan, J. Huang, Solvent annealing of perovskite-induced crystal growth for photovoltaic-device efficiency enhancement, *Adv. Mater.* 26 (2014) 6503–6509.
- [24] H. Huang, A.S. Susha, S.V. Kershaw, T.F. Hung, A.L. Rogach, Control of emission color of high quantum yield $\text{CH}_3\text{NH}_3\text{PbBr}_3$ perovskite quantum dots by precipitation temperature, *Adv. Sci.* (2015) 1–5, 1500194.
- [25] Y. Zhao, K. Zhu, Efficient planar perovskite solar cells based on 1.8 eV band gap $\text{CH}_3\text{NH}_3\text{PbI}_2\text{Br}$ nanosheets via thermal decomposition, *J. Am. Chem. Soc.* 136 (2014) 12241–12244.
- [26] J.H. Noh, S.H. Im, J.H. Heo, T.N. Mandal, S.I. Seok, Chemical management for colorful, efficient, and stable inorganic–organic hybrid nanostructured solar cells, *Nano Lett.* 13 (2013) 1764–1769.
- [27] K. Tanaka, T. Takahashi, T. Ban, T. Kondo, K. Uchida, N. Miura, Comparative study on the excitons in lead-halide-based perovskite-type crystals $\text{CH}_3\text{NH}_3\text{PbBr}_3$, $\text{CH}_3\text{NH}_3\text{PbI}_3$, *Solid State Commun.* 127 (2003) 619–623.
- [28] Q. Lin, A. Armin, R.C.R. Nagiri, P.L. Burn, P. Meredith, Electro-optics of perovskite solar cells, *Nat. Photon.* 9 (2015) 106–112.
- [29] T.-W. Lee, Y. Chung, O. Kwon, J.-J. Park, Self-organized gradient hole injection to improve the performance of polymer electroluminescent devices, *Adv. Funct. Mater.* 17 (2007) 390–396.
- [30] T.-H. Han, M.-R. Choi, S.-H. Woo, S.-Y. Min, C.-L. Lee, T.-W. Lee, Molecularly controlled interfacial layer strategy toward highly efficient simple-structured organic light-emitting diodes, *Adv. Mater.* 24 (2012) 1487–1493.
- [31] Y.-H. Kim, C. Wolf, H. Cho, S.-H. Jeong, T.-W. Lee, Highly efficient, simplified, solution-processed thermally activated delayed-fluorescence organic light-emitting diodes, *Adv. Mater.* 28 (2016) 734–741.
- [32] E. Edri, S. Kirmayer, M. Kulbak, G. Hodes, D. Cahen, Chloride inclusion and hole transport material doping to improve methyl ammonium lead bromide perovskite-based high open-circuit voltage solar cells, *J. Phys. Chem. Lett.* 5 (2014) 429–433.
- [33] N. Kitazawa, Y. Watanabe, Y. Nakamura, Optical properties of $\text{CH}_3\text{NH}_3\text{PbX}_3$ ($X = \text{halogen}$) and their mixed-halide crystals, *J. Mater. Sci.* 37 (2002) 3585–3587.
- [34] J.H. Heo, D.H. Song, S.H. Im, Planar $\text{CH}_3\text{NH}_3\text{PbBr}_3$ hybrid solar cells with 10.4% power conversion efficiency, fabricated by controlled crystallization in the spin-coating process, *Adv. Mater.* 26 (2014) 8179–8183.